Quantifying carbon-nanotube species with resonance Raman scattering

Quantifying carbon-nanotube species with resonance Raman scattering

A. Jorio,[1] A. P. Santos,[2] H. B. Ribeiro,[1] C. Fantini,[1] M. Souza,[1] J. P. M. Vieira,[1] C. A. Furtado,[2] J. Jiang,[3] R. Saito,[3]
L. Balzano,[4] D. E. Resasco,[4] and M. A. Pimenta[1]

[1]*Departamento de Física, Universidade Federal de Minas Gerais, Belo Horizonte, MG 30123-970, Brazil*
[2]*Centro de Desenvolvimento de Tecnologia Nuclear, Belo Horizonte, MG 30123-970, Brazil*
[3]*Department of Physics, Tohoku University and CREST JST, Aoba Sendai, 980-8578, Japan*
[4]*School of Chemical Engineering and Materials Science, University of Oklahoma,
Norman, OK 73019, USA*
(Received 23 March 2005; published 16 August 2005)

The method for quantifying the amount of each carbon nanotube specie, as defined by its diameter and chiral angle, as well as the semiconducting-to-metallic ratio in any type of carbon nanotube sample is discussed. Single-wall carbon nanotubes grown by the cobalt-molybdenum catalyst based (CoMoCAT) process are characterized. The semiconducting-to-metallic ratio is found to be 11:1. A single semiconducting specie, named the (6,5) nanotube represents 2/5 of the sample, while the most abundant metallic nanotube is the (7,4), which exhibits a diameter similar to the (6,5).

I. INTRODUCTION

Carbon nanotube samples generally exhibit many nanotube species, each specie being characterized by its diameter and chiral angle (d_t, θ), or equivalently by its (n,m) indices.[1–3] Large efforts are being directed to the controlled synthesis of single-wall carbon nanotube (SWNT) samples with well defined (n,m) species.[2] Particularly important is the separation of semiconducting and metallic SWNTs in a sample [SWNTs are metallic if $(2n+m)$ is a multiple of 3, and semiconducting otherwise[1–3]]. To be able to reach this goal, however, the development of methods able to quantify the species, i.e. to characterize the (n,m) sample population and to measure the semiconducting-to-metallic ratio are necessary. In this work, such a method is presented, based on the resonance Raman scattering process[4] with a quasicontinuous set of excitation laser lines. The method is used to characterize a SWNT sample grown by the cobalt-molybdenum catalyst-based (so-called CoMoCAT) process,[5] which exhibits evidence for being one of the most effective catalyst-based processes for highly selective SWNT growth.[6]

The method to quantify the (n,m) population by using the resonance Raman scattering method is based on the assumption that the intensity for the fully resonant Raman signal depends on the scattering efficiency (or Raman cross section) of the specific nanotube and on the number of scatterers, i.e., on the population of this specific tube in the sample. Therefore, by measuring the fully resonant Raman intensity for each specific nanotube in the sample, and correcting for the (n,m) dependent Raman cross section, the amount of each specie in the sample is obtained. To understand the method it is important to know how to measure and how to identify this "fully resonant Raman signal" for each specie. These procedures will be discussed here.

II. EXPERIMENTAL DETAILS

CoMoCAT SWNTs are synthesized at 750 °C using a silica-supported cobalt molybdenum catalyst and purified to remove the silica from the mixture, as described in Ref. 6. SWNT dispersions were prepared by adding the CoMoCAT tubes (0.6 mg/ml) to an aqueous solution containing the surfactant sodium dodecyl sulfate [SDS, $(CH_3(CH_2)11-OSO3Na)$] at 0.4 wt. %. The mixture was homogenized using a magnetic stirrer and adjusted to a pH of 10 using a concentrated NaOH solution. Sonication was carried out for 15 min in an ultrasonic bath at a power level of 40 W. This suspension was then centrifuged in an Eppendorf 5417C centrifuge for 15 min at 20600 g to separate larger particles or bundled tubes from the lower density surfactant-suspended individual nanotubes. Finally, samples of as-grown purified material and the supernatant liquid enriched in debundled surfactant-suspended SWNTs, as well as a solid SWNT +SDS sample after precipitation and another sample after drying the solution, were withdrawn for Raman studies.

The spectra were obtained at room temperature with a Dilor XY triple-monochromator equipped with a microscope and a CCD detector. The sample was excited using Ar-Kr and dye lasers. The Raman spectrum of CCl_4 was measured after each RBM measurement and is used for intensity and frequency calibration.

III. RESULTS AND DISCUSSIONS

Figures 1(A)–1(C) show resonance Raman intensity maps for the nanotube radial breathing modes (RBM) obtained (A) from the as-grown purified sample, (B) from the SWNT +SDS solution, and (C) from the SWNT+SDS precipitate, as a function of the excitation laser energy (E_{laser}). The RBM frequency (ω_{RBM}) depends on the specific nanotube structure,[1–4] and the ω_{RBM} to (n,m) relation is established within experimental precision (± 1 cm^{-1} accuracy) for HiPco SWNTs in solution.[7] The RBM intensities also depend on the specific nanotube, since the Raman cross section increases by about three orders of magnitude when full resonance is achieved, i.e., when E_{laser} matches the optical transition energy of a specific nanotube.[1–4] Each nanotube has a different
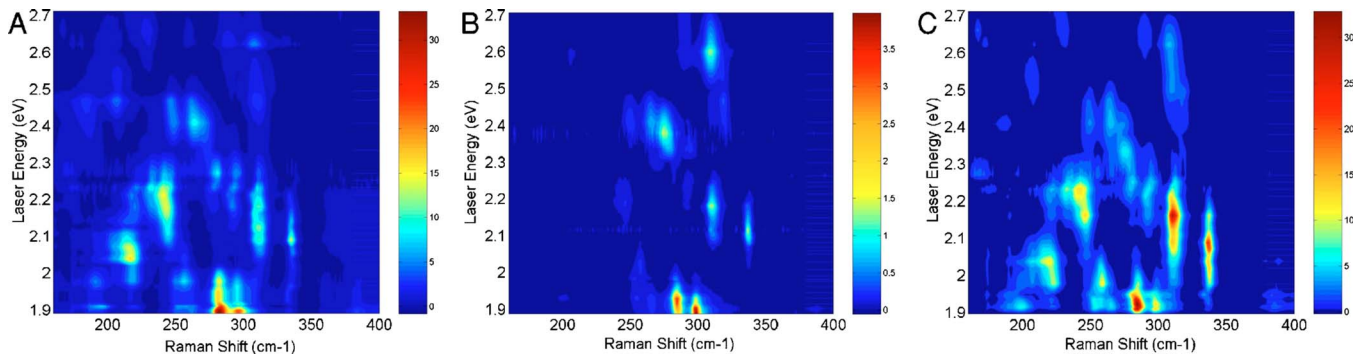
FIG. 1. (Color online) RBM spectra vs E_{laser} for CoMoCAT SWNT samples. A, B, and C stand for the as-grown purified sample, the SWNT+SDS solution sample, and the SWNT+SDS precipitate sample, respectively. The Raman intensity is given by different colors, as shown in the intensity bars on the right (arb. units). The horizontal traces on the right-hand side of the 2D maps give the excitation laser energies that have been used to produce these maps. The union of spectral profiles is made within the MatLab interpolation process.

optical transition energy (E_{ii}, where $i = 1, 2, \ldots$ numbers the 1st, 2nd,… optical transition energies), so that fully resonant Raman scattering for each (n, m) tube occurs for different E_{laser} values. Such an effect is clearly seen in Figs. 1(A)–1(C), where each RBM peak increases and decreases in intensity with increasing laser energy as the related (n, m) SWNT enters and leaves resonance with the excitation laser line. Theoretical models describing the relation between E_{ii} and (n, m) within experimental precision (± 10 meV accuracy) have already been developed for HiPco SWNTs in solution.[7–9] Therefore, by identifying the RBM intensity for each specific (n, m) nanotube in Fig. 1 and correcting for the (n, m) dependent Raman cross section, the amount of each nanotube in the sample can be obtained.

For the (n, m) assignment of the RBM Raman signals in Fig. 1, we consider Fig. 2(A), which plots the electronic transition energies (E_{ii}) as a function of the RBM frequencies (ω_{RBM}) for each (n, m) SWNT,[7,9] in the ω_{RBM} and E_{laser} ranges where the experiments were performed. Note the formation of family patterns (lines connecting data points) for SWNTs with $2n + m = $ constant that drives the (n, m) assignments.[1,10–12] By comparing the geometrical patterns in Fig. 2(B) with Fig. 2(A), the resonances with E_{22}^S, E_{11}^M, E_{33}^S (S and M superscript stand for semiconducting and metallic SWNTs, respectively) can be identified [see white ellipses in Fig. 2(B)], and even the E_{44}^S optical transitions can be assigned. The E_{44}^S RBM peaks are not clear in Figs. 1 and 2(B) but they are observable in the raw data.

The general results are consistent for the SWNT samples in solution and in solid form (as-grown, precipitate, and after drying the solution), although some differences in relative intensities are observed. The greatest intensity difference is observed when comparing the 2D Raman plot in solid samples versus solution. In the solution sample, the Raman signal from RBMs below 250 cm^{-1}, i.e., from SWNTs with d_t above ~0.94 nm [see Ref. 7 for the ω_{RBM} dependence on (d_t, θ)] are much weaker than the Raman signals for RBMs above 250 cm^{-1} ($d_t < 0.94$ nm), while in the solid samples the intensities are more homogeneous [compare Figs. 1(A) and 1(C) with 1(B)]. Figure 2(B) shows the same plot as in Fig. 1(B), but now using a logarithmic intensity scale to clearly show the presence of very weak RBM peaks for
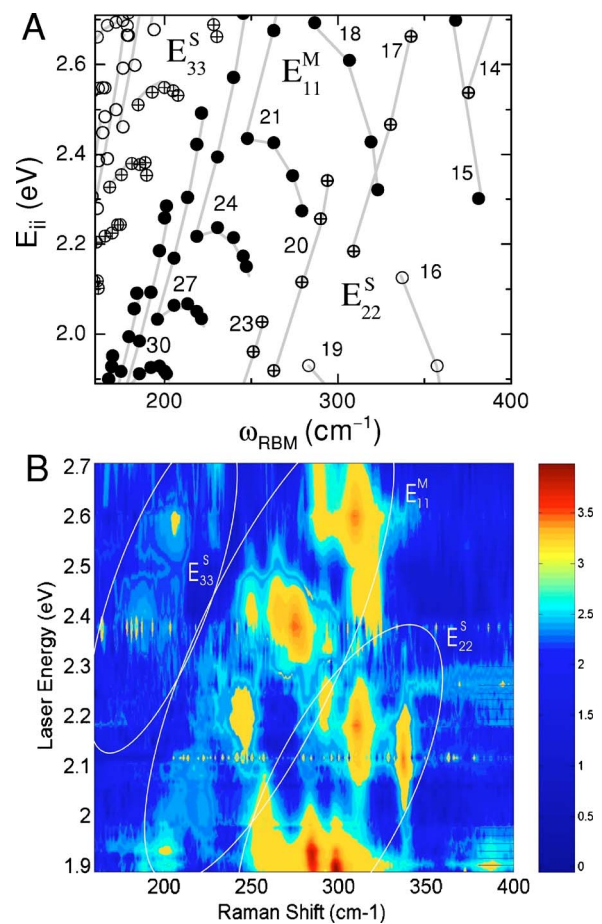

FIG. 2. (Color online) (A) E_{ii} vs ω_{RBM} plot based on an extended tight binding model (Ref. 9) and corrections to account for many-body effects (Ref. 7). Solid, open, and crossed symbols stand for (n, m) SWNTs with $(2n + m) \bmod 3 = 0$ (metallic), 1 or 2 (semiconducting) SWNTs, respectively. The gray lines connect SWNTs within the same $(2n + m)$ family. The $(2n + m)$ numbers are displayed close to each family. (B) A plot similar to Fig. 1(B), but now with a color pattern that follows a log scale (see change in the intensity bar) to clearly show the low intensity RBM peaks. The white ellipses define the ranges where E_{22}^S, E_{11}^M, and E_{33}^S optical transitions are observed.

larger diameter tubes. These intensity differences between the solid and solution samples can be due either to the decrease of the population of larger diameter tubes in the solution sample, or due to the decrease of the population of small diameter tubes in the solid samples. The first process was seen on DNA wrapped samples,[13] and ascribed to a diameter selective wrapping process. The second process can be identified here since the intensity ratio for large to small diameter tubes increases with increasing laser power in an irreversible way, in all solid samples (as-grown, precipitate, and after drying the solution), suggesting the burning of the more reactive small diameter tubes in the solid samples. This effect does not happen in the solution where the heat exchange with the solvent is efficient, and high power (up to 20 mW on a 50× objective) can be applied with no change in the spectral profile. More systematic work is needed for clarifying the effect of laser power and manipulation processes on the (n,m) population, and such a study can be performed with the method presented here.

The spectral linewidths (FWHM) for the RBM features (γ_{RBM}) and for the resonance energy windows (γ_r) in the solid samples are broadened with respect to the solution, with average values of $\gamma_{RBM}=7$ cm^{-1} and $\gamma_r=100$ meV for the purified sample, and $\gamma_{RBM}=5$ cm^{-1} and $\gamma_r=40$ meV for the sample in solution. The γ_r and γ_{RBM} for the precipitate and dried SWNT+SDS samples are in between the values for the as-grown and solution samples. Note that the resonance linewidths are in the same order of magnitude (tens of meV) as the changes in E_{ii} values due to environmental effects.[11,13–15] Therefore, the determination of the (n,m) population through resonance Raman intensity analysis using a single excitation laser line is not accurate, unless the effect of the environment and the position of E_{ii} is known precisely. This problem does not happen when using a quasicontinuous set of excitation laser lines, since full resonance can always be achieved. The experimental procedure presented here can also be used to characterize the environmental effects on the E_{ii} energies.[11,13,15]

By comparing the intensity profiles in Figs. 1(A), 1(C), and 2(B) with Fig. 2(A), the metallic SWNTs can be assigned. Metallic tubes belonging to the families $(2n+m)$ =18, 21, 24, 27, and 30 can be observed, as shown by the five sets of peaks inside the E_{11}^M energy region in Fig. 2(B), around 2.6, 2.4, 2.2, 2.05 (relatively weak) and 1.95 eV, respectively. Although two E_{11}^M are predicted by theory [see filled circles in Fig. 2(A)], only the low energy E_{11}^M component is observed for the CoMoCAT SWNT samples, consistent with measurements in HiPco samples.[11]

The analysis of the resonance profiles, i.e., the RBM Raman intensities (I_{RBM}) as a function of E_{laser}, gives the maximum resonance Raman RBM integrated intensity (I_{RBM}^{EXP}) for each (n,m) SWNT under full resonance conditions. Within the energy and diameter range measured here, 24 metallic and 42 semiconducting SWNTs are expected to be in resonance, with the semiconducting to metallic population ratio of S:M=1.75 [if the (n,m) population is homogeneous], that is close to 2, the value that would be obtained if all the possible (n,m) SWNTs were present homogeneously. Raman signals from only 17 metallic and 27 semiconducting

TABLE I. The (n,m), $2n+m$ family number, diameter d_t $=0.142\sqrt{n^2+m^2+nm}\sqrt{3}/\pi$ (nm), chiral angle θ (deg), E_{ii} (eV) (Ref. 7), ω_{RBM} (cm^{-1}), measured RBM intensity I_{RBM}^{EXP} (normalized), calculated intensity I_{RBM}^{CALC} (arb. unit) (Ref. 16, [17]), and population $P=I_{RBM}^{EXP}/I_{RBM}^{CALC}$ (normalized), for semiconducting and metallic Co-MoCAT SWNTs in solution. The results are obtained by fitting all the spectra with a sum of Lorentzians. The I_{RBM}^{EXP} and P values are normalized to give 100 to the largest values.

(n,m)	$2n+m$	d_t	θ	E_{22}^S	ω_{RBM}	I_{RBM}^{EXP}	I_{RBM}^{CALC}	P
(6,4)	16	0.68	23.4	2.11	337	21.9	0.94	7.9
(6,5)	17	0.75	27.0	2.18	309	42.5	0.14	100.0
(7,5)	19	0.82	24.5	1.92	284	85.7	0.57	51.2
(7,6)	20	0.88	27.5	1.92	266	7.0	0.08	28.9
(8,3)	19	0.77	15.3	1.86	299	100.0	1.32	25.7
(9,2)	20	0.79	9.8	2.24	291	4.3	0.34	4.2
(10,3)	23	0.92	12.7	1.95	254	6.0	0.22	9.4
(11,1)	23	0.90	4.3	2.03	259	6.3	0.50	4.3

(n,m)	$2n+m$	d_t	θ	E_{11}^M	ω_{RBM}	I_{RBM}^{EXP}	I_{RBM}^{CALC}	P
(6,6)	18	0.81	30.0	2.69	288	5.65	2.83	0.7
(7,4)	18	0.75	21.1	2.61	308	31.75	1.93	5.6
(7,7)	21	0.95	30.0	2.43	250	4.32	1.74	0.8
(8,2)	18	0.72	10.9	2.43	318	10.86	2.99	1.2
(8,5)	21	0.89	22.4	2.43	265	9.68	1.24	2.6
(9,3)	21	0.85	13.9	2.35	274	12.98	2.19	2.0
(9,6)	24	1.02	23.4	2.24	233	1.14	0.84	0.5
(9,9)	27	1.22	30.0	2.03	198	0.41	0.77	0.2
(10,1)	21	0.82	4.7	2.27	280	21.62	2.76	2.6
(10,4)	24	0.98	16.1	2.22	242	2.79	1.54	0.6
(10,7)	27	1.19	24.2	2.07	204	0.41	0.60	0.2
(11,2)	24	0.95	8.2	2.19	245	8.54	2.13	1.4
(11,5)	27	1.11	17.8	2.06	215	0.57	1.10	0.2
(12,0)	24	0.94	0	2.16	247	3.43	2.36	0.5
(12,3)	27	1.08	10.9	2.04	220	0.92	1.62	0.2
(13,1)	27	1.06	3.7	2.02	224	1.08	1.93	0.2
(14,2)	30	1.18	6.6	1.92	202	3.43	1.54	0.8

SWNTs were observable here. By summing up the maximum RBM intensities from all the metallic and semiconducting SWNTs in the solution and in the as-grown purified samples, the semiconducting to metal signal ratios S:M(solution) =2.4 and S:M(as grown)=1.2 are obtained. The differences are due to the predominance of Raman signal from small diameter semiconducting SWNTs in the solution. Before deriving any conclusion about the S:M population ratio in the samples, however, the S:M signal ratio data obtained above need to be corrected by the (n,m)-dependent Raman cross-section values.[16,17] The analysis developed further for the (n,m) dependent Raman intensities and populations will be based on the experimental results from the solution, first because the sample is homogeneous and easier to control thermal effects, and second because the Raman results for semiconducting SWNTs can be directly compared with published photoluminescence results.[6]

The maximum RBM intensities (I_{RBM}^{EXP}) can now be analyzed as a function of (n,m). The results are displayed in Table I for the eight signals for semiconducting SWNTs in resonance with E_{22}^S, and for the 17 metallic SWNT features clearly observed in solution. Raman signals from semiconducting SWNTs in resonance with E_{33}^S and E_{44}^S were considered for determining the S:M signal ratio, but they are not included in Table I. It is hard to assign (n,m) values for E_{33}^S and E_{44}^S resonant tubes because the Raman signals from different (n,m) are too close in Raman frequency and resonance energy (they all together account for less than 10% of the RBM Raman signal anyway). The results in Table I are normalized so that $I_{RBM}^{EXP}=100$ for the highest intensity RBM peak. Since the electron-phonon coupling exhibits a strong (n,m) dependence,[16–18] in order to characterize the population of specific (n,m) SWNTs in each sample, the RBM resonance intensities have to be analyzed considering the (n,m) dependence of the RBM Raman cross section. This (n,m) dependent RBM intensity is given by I_{RBM}^{CALC} in Table I. The I_{RBM}^{CALC} was calculated here by using the procedure discussed in Refs. 16,[17], and making use of the recently developed models that describe the nanotube physics, taking into account the curvature effects.[9] We expect the ratio $P=I_{RBM}^{EXP}/I_{RBM}^{CALC}$ given in Table I to reflect the population of each specific (n,m) SWNT within the samples. The populations (intensity ratios) were also normalized to give 100 for the highest P value, i.e., for the (6,5) SWNT. By summing up all the population results, the P value can be seen as the number of each specific (n,m) nanotube in an ensemble of 250 nanotubes.

By analyzing the P given in Table I, it is clear that the semiconducting (6,5) SWNT is the most abundant. It represents about 2/5 of the sample. The P are also large for the (7,5), (7,6), and (8,3) tubes. These results are in agreement with photoluminescence experiments in the CoMoCAT sample after dispersion and sonication of the SWNTs in aqueous solution with SDS.[6] The photoluminescence technique is limited to semiconducting tubes and, even for semiconducting tubes, they are not luminescent in their usually as-grown bundled form. Nevertheless the photoluminescence results can be used here to validate the Raman results for semiconducting SWNTs+SDS in solution. From P obtained by RRS, we can estimate that ~60% of the sample is composed of the (6,5) and (7,5) tubes, which is in good agreement with photoluminescence results.[6] Note that while the largest $P=100$ value was obtained for the (6,5) SWNT in all three samples in Fig. 1, the largest observed RBM intensity values ($I_{RBM}^{EXP}=100$) occur for the (8,3) SWNTs (see Table I). The consistency between the corrected population values P and the photoluminescence results[6] for semiconducting nanotubes in solution confirms the validity of the I_{RBM}^{CALC} calculation and the importance of correcting the I_{RBM}^{EXP} for the (n,m) dependent Raman cross section.

All RBM intensity ratios (P) in Table I are plotted in Fig. 3 as a function of diameter and chiral angle. The P for metallic tubes are multiplied by 10 to be clearly observed in Fig. 3. By summing up all the P for semiconducting and metallic tubes a S:M ratio of 11:1 is obtained.

The left panel in Fig. 3 shows a sharp diameter selectivity for the CoMoCAT process (sharper than for SWNT tubes
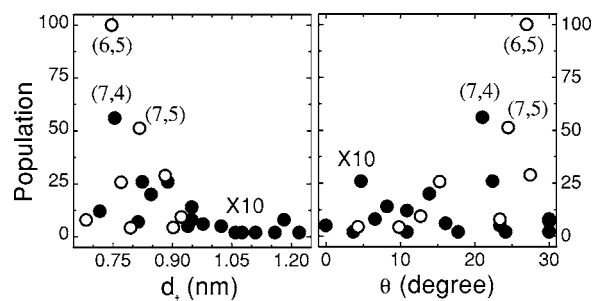

FIG. 3. The (n,m) dependent populations (P) vs diameter (left) and chiral angle (right) for various CoMoCAT SWNTs. Filled and open circles stand for metallic and semiconducting SWNTs, respectively. The P values for metallic SWNTs are multiplied by 10 to more clearly relate their d_t and θ behavior to that for semiconducting SWNTs. The (n,m) for the most intense P values are given.

grown by the HiPco process[7,10]), being applicable to both semiconducting (solid circles) and metallic (open circles) SWNTs. The right panel in Fig. 3 shows the selectivity for large chiral angle SWNTs in this synthesis process [consistent with results for small diameter HiPco SWNTs (Ref. 7)]. Particularly interesting is the largest P value observed for the (7,4) metallic SWNTs in solution—see bright spot at $E_{11}^M=2.61$ eV and $\omega_{RBM}=308$ cm^{-1} in Fig. 1(B). Thus, the most abundant metallic tube, the (7,4) has almost the same ω_{RBM} value, i.e., the same diameter as the most abundant semiconducting SWNT, the (6,5) tube.

IV. SUMMARY AND FINAL DISCUSSION

The experimental procedure for the characterization of the semiconducting to metallic ratio and the (n,m) population is here established. This procedure has the advantage over photoluminescence experiment for being applicable to SWNTs in bundles, and for measuring metallic tubes as well. The experimental precision of this method is given by the experimental precision for determining the resonance Raman intensity for each RBM signal. This precision depends on the signal-to-noise level and on the spacing between excitation laser lines, and these precision parameters are different for different (n,m) SWNTs. In our case, the overall experimental precision on population determination varies from 1% to 20% of the specified result.

While determination of the most abundant tube, namely the (6,5) tube, is in agreement with photoluminescence experiments, the precise population characterization obtained here depends on the calculated results for the (n,m) dependence of the Raman intensity. The accuracy for the intensity calculation depends on the accuracy of the matrix element calculation. The present matrix elements have explicitly considered curvature effect,[7–9] they agree well with the matrix elements obtained by other methods,[17,18] and the accuracy is larger than the numbers we give in Table I. Of course the very precise value depends on the physical assumptions, since we must know all the physics behind the scattering event. For the moment we believe that what we present is a

combination of the best results that can be prepared with the present knowledge. Since there is no available sample with a well known (n,m) population to validate the theoretical calculations for the resonance Raman (and photoluminescence) efficiency, comparison between resonance Raman spectroscopy and photoluminescence performed on the same sample provide a self-consistent way to check the theories. Such a comparison is not possible for metallic tubes, but in principle there is no reason why the Raman scattering effect should be different in metallic and semiconducting SWNTs, unless conduction electrons play some role.

The experimental procedure presented here is capable, therefore, of accurately characterizing the different synthesis and manipulation processes, such as wrapping and bundling. For example, two RBM features spaced by 2.3 cm^{-1} can be clearly observed in Raman experiments with high dispersion setukp for the (6,5) SWNT.[19] Small changes in the electronic transition energies (below 0.1 eV) and populations are clearly observed when comparing different samples. These details will be published elsewhere with more systematic analysis.

[1] R. Saito, G. Dresselhaus, and M. S. Dresselhaus, *Physical Properties of Carbon Nanotubes* (Imperial College, London, 1998).

[2] M. S. Dresselhaus, G. Dresselhaus, and Ph. Avouris, *Springer Series in Topics in Applied Physics* (Springer-Verlag, Berlin, 2001), Vol. 80.

[3] S. Reich, C. Thomsen, and J. Maultzsch, *Carbon Nanotubes: Basic Concepts and Physical Properties* (Wiley-VCH, Berlin, 2004).

[4] A. M. Rao, E. Richter, S. Bandow, B. Chase, P. C. Eklund, K. W. Williams, S. Fang, K. R. Subbaswamy, M. Menon, A. Thess, R. E. Smalley, G. Dresselhaus, and M. S. Dresselhaus, Science **275**, 187 (1997).

[5] B. Kitiyanan, W. E. Alvarez, J. H. Harwell, and D. E. Resasco, Chem. Phys. Lett. **317**, 497 (2000).

[6] S. M. Bachilo, L. Balzano, J. E. Herrera, F. Pompeo, D. E. Resasco, and R. B. Weisman, J. Am. Chem. Soc. **125**, 11186 (2003).

[7] A. Jorio, C. Fantini, M. A. Pimenta, R. B. Capaz, G. G. Samsonidze, G. Dresselhaus, M. S. Dresselhaus, J. Jiang, N. Kobayashi, A. Gruneis, and R. Saito, Phys. Rev. B **71**, 075401 (2005).

[8] V. Popov, New J. Phys. **6**, 17 (2004).

[9] Ge. G. Samsonidze, R. Saito, N. Kobayashi, A. Grüneis, J. Jiang, A. Jorio, S. G. Chou, G. Dresselhaus, and M. S. Dresselhaus, Appl. Phys. Lett. **85**, 5703 (2004).

[10] S. M. Bachilo, M. S. Strano, C. Kittrell, R. H. Hauge, R. E. Smalley, and R. B. Weisman, Science **298**, 2361 (2002).

[11] C. Fantini, A. Jorio, M. Souza, M. S. Strano, M. S. Dresselhaus, and M. A. Pimenta, Phys. Rev. Lett. **93**, 147406 (2004).

[12] H. Telg, J. Maultzsch, S. Reich, F. Hennrich, and C. Thomsen, Phys. Rev. Lett. **93**, 177401 (2004).

[13] S. G. Chou, H. B. Ribeiro, E. B. Barros, A. P. Santos, D. Nezich, Ge. G. Samsonidze, C. Fantini, M. A. Pimenta, A. Jorio, F. Plentz Filho, M. S. Dresselhaus, G. Dresselhaus, R. Saito, M. Zheng, G. B. Onoa, E. D. Semke, A. K. Swan, M. S. Ünlü, and B. B. Goldberg, Chem. Phys. Lett. **397**, 296 (2004).

[14] J. Lefebvre, J. M. Fraser, and Y. Homma *et al.*, Appl. Phys. A: Mater. Sci. Process. **78**, 1107 (2004).

[15] M. J. O'Connell, S. Sivaram, and S. K. Doorn, Phys. Rev. B **69**, 235415 (2004).

[16] J. Jiang, R. Saito, A. Gruneis, S. G. Chou, G. G. Samsonidze, A. Jorio, G. Dresselhaus, and M. S. Dresselhaus, Phys. Rev. B **71**, 205420 (2005).

[17] V. N. Popov, L. Henrard, and P. Lambin, Nano Lett. **4**, 1795 (2004).

[18] M. Machón, S. Reich, H. Telg, J. Maultzsch, P. Ordejón, and C. Thomsen, Phys. Rev. B **71**, 035416 (2005).

[19] A. Jorio, C. Fantini, L. G. Canado, H. B. Ribeiro, A. P. Santos, C. A. Furtado, M. S. Dresselhaus, G. Dresselhaus, Ge. G. Samsonidze, S. G. Chou, A. Grueneis, J. Jiang, N. Kobayashi, R. Saito, and M. A. Pimenta, in *Proceedings of the International Winterschool on Electronic Properties of Novel Materials*, Kirchberg, Austria, 12–19 March 2005.